DELPHI 97-72 CONF 58
28 July, 1997

Investigation of the Splitting of Quark and Gluon Jets

Preliminary

DELPHI Collaboration

K. Hamacher, O. Klapp and P. Langefeld
University of Wuppertal, Germany

Abstract

The splitting processes in identified quark and gluon jets are investigated using longitudinal and transverse observables. The jets are selected from symmetrical three-jet events measured in Z decays with the DELPHI detector. Gluon jets are identified using heavy quark anti-tagging.

Scaling violations in identified gluon jets are observed for the first time. The ratio of the energy dependence of the fragmentation functions is found to be $2.8 \pm 0.8_{stat}$ consistent with the QCD expectation.

The maximum of the ratio of the primary splitting probabilities in quark and gluon jets is measured to be $\tilde{r}_1^{max} = 3.2 \pm 0.2_{stat}$ in agreement with QCD models.

The azimuthal distributions of the subjets in gluon and quark jets provide evidence for a depletion of the primary gluon splittings at large y. The investigation of higher rank splittings shows that this depletion is conserved in the further jet evolution and consequently is the reason for the observed small charged hadron multiplicity ratio in gluon to quark jets.

Paper submitted to the LP'97 Conference
Hamburg, July 28 - August 1st

1 Introduction

The dynamics of the strong interaction is described by Quantum Chromodynamics, QCD, a non-abelian gauge theory. This theory contains two types of fundamental fields, the fermionic quarks and the self-interacting gluons, the vector bosons mediating the strong force. Quarks and gluons are not directly observed; however they give rise to narrow bunches of hadrons called jets. In our present understanding those jets result from a showering process, a chain of elementary splitting processes of the initial quarks or gluons. The relative coupling strength of these splittings is determined by the so-called QCD colour factors, $C_F = \frac{4}{3}$, $C_A = 3$ and $T_F = \frac{1}{2}$. C_F determines the coupling of a gluon to a quark, C_A the gluon self-coupling and T_F the splitting of a gluon into a quark-antiquark pair. The latter process is kinematically suppressed.

Stronger splittings are thus expected in gluon jets compared to quark jets as $\frac{C_A}{C_F} = \frac{9}{4}$. Consequently gluon jets and quark jets should be substantially different. In particular one naïvely expects the ratio $\frac{n_g}{n_q}$ of the hadron multiplicities in gluon to quark jets to be approximately $\frac{C_A}{C_F}$ [1]. This expectation is essentially maintained in more elaborate calculations [2].

Experimentally, however, the observed differences in quark and gluon jets are small [4, 3]. In three-jet events in e^+e^- - annihilation at Z energies, n_g/n_q is measured to be about 1.25 [4, 3]. However, in a previous paper [4] an increase of this ratio with energy was demonstrated. Subsequently this observation has been confirmed by new results [5].

It is important to clarify the origin of the obvious discrepancy of the experimental findings and expectation. This may also help explain why differences between quark and gluon jets in e^+e^- - annihilation are small.

Quark and gluon jets are selected in planar symmetric three-jet events. Gluon jets are identified using heavy quark tagging. The definition of a quark or gluon jet relies on the analogy to tree level graphs. Higher order corrections affect this identification by terms of $\mathcal{O}(\alpha_S)$. As the interest of this paper is mainly to achieve qualitative understanding, these subtleties are ignored.

The aim of this paper is

- to establish that the initial splittings in quark and gluon jets are indeed consistent with the QCD expectations; and
- to study the further jet evolution in order to understand and explain the observed small difference in particle multiplicity in quark and gluon jets.

To achieve these objectives, two different types of observables are used. These are the scale dependence of the stable hadron scaled energy, sensitive mainly to the longitudinal part of the jet evolution; and the subjet rates as defined by the Durham jet finder related to the transverse momentum of the splitting process ($k_t \approx E_{vis} \cdot \sqrt{y_{cut}}$). In addition the azimuthal distribution of the subjets with respect to the event plane is analysed.

The paper is organized as follows. Section 2 describes the parts of the DELPHI detector relevant to this analysis, the track and event selection, the jet reconstruction and the impact parameter tagging used to antitag gluon jets and heavy quark events, as well as the subtraction method used to obtain properties of pure quark and gluon jets. Section 3 contains some theoretical preliminaries and introduces the variables and distributions used to study the jet splittings. The results are presented in section 4. Conclusions appear in section 5.

2 Experimental Apparatus and Event Selection

2.1 The Delphi Detector

A detailed description of the DELPHI apparatus has been presented in [6]. Here the components relevant for this analysis are briefly described.

The main part of the tracking system is a 2.7 m long Time Projection Chamber (TPC) which measures the tracks of charged particles with a resolution of about 250 μm in the $R\phi$-projection (transverse to the beam direction) and 0.9 mm along the z direction (beam direction). The space between the TPC and the beam pipe contains the Inner Detector (ID) and a silicon microstrip Vertex Detector (VD). Each 15° sector of the ID consists of a 24 wire jet chamber followed by a 5 layer proportional chamber. The Vertex Detector consists of three concentric shells of 24 silicon microstrip detector modules each 24 cm long. It has very good spatial resolution and is therefore the most important detector component of DELPHI for the reconstruction of vertices and for the impact parameter tag. In the barrel region (polar angle θ relative to the beam axis between 43° and 137°), the quality of tracking is further improved by the Outer Detector containing 5 layers of drift tubes. Each layer measures the $R\phi$-coordinate with a resolution of about 110 μm. Three layers also provide an approximate z measurement.

In the forward and backward regions (θ in the range $11° - 33°$ or $147° - 169°$), two additional drift chamber systems improve the tracking. Forward chamber A (FCA) consists of three pairs of wire planes rotated by 120° with respect to each other, in order to resolve ambiguities internally. Forward chamber B (FCB) consists of 12 wire planes twice repeating the orientation of FCA and positioned directly in front of the forward electromagnetic calorimeter ($FEMC$).

Electromagnetic clusters are measured in the barrel region by a High Density Projection Chamber (HPC) and in the forward region (θ in the range $10° - 36.5°$ or $143.5° - 170°$) by the $FEMC$, a matrix of 4522 lead glass blocks. The HPC consists of 144 modules arranged in 6 rings around the beam axis. It achieves good two-shower separation, due to a 3 dimensional measurement of the shower profile. The Hadron Calorimeter (HAC) provides energy and position measurements for neutral hadrons.

2.2 Event Selection

All data collected by DELPHI during the years 1991 to 1994 are considered in the present analysis. In a first step of the selection procedure, quality cuts on all charged particles and all neutral clusters in the calorimeters are imposed in order to ensure a reliable determination of their momenta, energies, and multiplicities. The quality cuts for charged and neutral particles are given in table 1 and 2 respectively (ϵ is the impact parameter with respect to the primary vertex, L_{track} the measured track length).

All charged particles are assumed to be pions and all neutral particles are assumed massless. A sample of hadronic events is then selected as in [4, 7] by demanding a minimum charged multiplicity and visible energy, as well as requiring that events are well contained within the detector volume. The corresponding cuts are shown in table 3. ($E_{ch.}^{hemi}$ denotes the sum of the energies of charged particles in the forward or backward hemisphere of the DELPHI detector.)

Variable	Cuts
p	≥ 0.4 GeV/c
θ_{polar}	$20^\circ - 160^\circ$
ϵ_{xy}	$\leq 5.0\ cm$
ϵ_z	$\leq 10.0\ cm$
L_{track}	$\geq 30\ cm$
$\frac{\Delta p}{p}$	$\leq 100\%$

Table 1: Track cuts

Detector	E_{min} [GeV]	E_{max} [GeV]
HPC	0.5	50
EMF	0.5	30
HAC	1.0	50

Table 2: Energy cuts for neutral particles

Variable	Cut
$E_{ch.}^{hemi}$	$\geq 3\%\ \sqrt{S}$
$E_{ch.}^{tot}$	$\geq 15\%\ \sqrt{S}$
$N_{ch.}$	≥ 5
$\theta_{Shpericity}$	$30^\circ - 150^\circ$
max p	45 GeV/c

Table 3: Event cuts

2.3 The Jet Finding Algorithm

A three-jet event sample is selected using the $k_\perp$ jet clustering algorithm [8], originally known as the Durham jet finder. In this scheme, a jet resolution variable y_{ij} is defined for every pair of particles i and j in an event by:

$$y_{ij} \quad = \quad \frac{2 \cdot \min\left(E_i^2, E_j^2\right) \cdot (1 - \cos\Theta_{ij})}{E_{vis}^2}$$

where E_i and E_j are the energies of particles i and j, Θ_{ij} is the angle between their tracks and E_{vis} the sum of all measured particle energies in the event. The particle pair with the lowest value y_{ij} is selected and replaced by a pseudo-particle with the sum of their four-momenta, $p_{ij} = p_i + p_j$, if y_{ij} is below y_{cut}.

In successive steps the procedure is repeated, with the jet resolution variable being re-evaluated in each iteration, until all pairs i and j satisfy $y_{ij} > y_{cut}$. Each four-momentum vector which remains at the end of this process is referred to as a "jet". With this algorithm, the minimum transverse momentum between two jets, resolved at a scale defined by y_{cut}, is approximately given by $k_\perp^{min} \simeq E_{vis}\sqrt{y_{cut}}$.

The $k_\perp$ algorithm conserves both energy and momentum, is well suited for perturbative calculations and avoids the recombination of soft gluons in different hemispheres of the event.

2.4 Event Topologies

After the events have passed the hadronic event selection, the $k_\perp$ cluster algorithm is applied to select three-jet final states. This selection is carried out at a jet resolution scale $y_0 = 0.015$; this value maximizes the three-jet event sample and allows reliable comparison with perturbative QCD.

For a detailed comparison of quark and gluon jet properties it is necessary to obtain samples of quark and gluon jets with nearly the same kinematics, which allow a direct comparison of the jet properties within a similar environment. To fulfill this condition, different event topologies have been used, as illustrated in figure 1:

- mirror symmetric events, $\theta_2, \theta_3 \in [150^\circ - 15^\circ, 150^\circ + 15^\circ]$, subsequently called **Y events**
- three-fold symmetrical events, $\theta_2, \theta_3 \in [120^\circ - 15^\circ, 120^\circ + 15^\circ]$, subsequently called **Mercedes events**.

The jet axes are projected into the event plane, which is defined as the plane perpendicular to the smallest sphericity eigenvector as obtained from the quadratic momentum

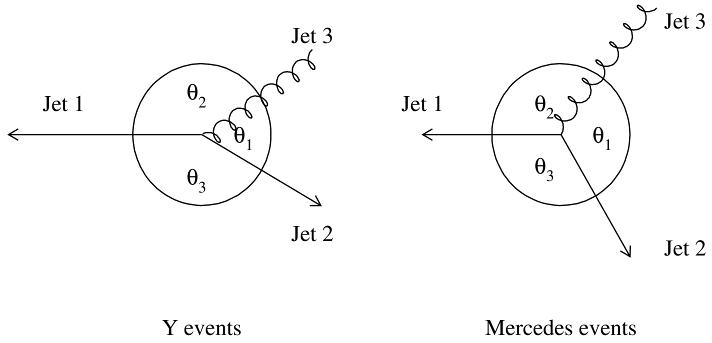

Figure 1: Event topologies of symmetrical Y events and Mercedes events. θ_i are the angles between the jets after projection into the event plane.

tensor. The jets are numbered in decreasing order of jet energy, where to each of the jets a calculated energy is assigned as derived from the angles between the jets. Assuming massless kinematics, the jet energy can be expressed as:

$$E_j^{calc} = \frac{sin\theta_j}{sin\theta_1 + sin\theta_2 + sin\theta_3}\sqrt{s}, \quad j = 1, 2, 3\,, \tag{1}$$

where θ_j is the interjet angle as defined in figure 1.

In order to enhance the contribution from events with three well-defined jets attributed to $q\bar{q}g$ production, a set of further cuts is applied to the three-jet event samples, as summarized in table 4. These cuts select planar events with each of the reconstructed jets well contained within the sensitive part of the detector.

Measurement	Symmetrical topologies
Number of particles in each jet	≥ 2 (charged or neutral)
Visible jet energy	≥ 5 GeV
Sum of angles between jets	$\geq 355°$
Polar angle of each jet axis	$30° - 150°$

Table 4: Planarity and acceptance cuts for reconstructed jets.

From the initial ~2,950,000 hadronic events collected by DELPHI in 91-94 and from ~6,360,000 Monte Carlo events, the numbers of events remaining after this selection procedure are given in table 5. In the case of Y events, the gluon jet can be compared to one quark jet, and for Mercedes events to two quark jets.

2.5 Lifetime Tag on Event and Jet Level

The lifetime signed impact parameter is used to construct an algorithm for tagging b jets. In this method the probability P_N to contain no decay products from long lived hadrons

	Y events		Mercedes events	
Year	Data	Monte Carlo	Data	Monte Carlo
1991	12610	18819	1368	2118
1992	35460	117152	3815	13787
1993	35748	97707	3948	10628
1994	69251	251618	7735	28236
total	153069	485296	16866	54769

Table 5: Event samples of the selected event topologies

(i.e. the probability that all tracks come directly from the e^+e^- - annihilation point) is evaluated for a given selection of N tracks. Thus events containing b quarks tend to give low values of P_N. Only events with a b quark signature are selected as input to the gluon identification by demanding that P_N, for the whole event, does not exceed a value of 0.032. The tracks corresponding to each of the reconstructed jets are used to construct a probability P_J per jet. Jets are finally classified according to the observed values of each P_J following two selection strategies:

I. As the most energetic jet in Y events is a quark jet in about 98% of the cases, this jet is treated as a quark jet in every Y event. Cuts on P_J are applied to each of the two lower energy jets in order to establish which is the quark and which is the gluon jet. The main criterion applied is to demand that one of the two lower energy jets satisfies the condition $P_J < 0.1$. The remaining jet is then taken as the gluon provided its probability value P_J does not fall below 0.1. This latter cut ensures that the decay products of the b hadrons do not, in general, filter through to the selected sample of gluon jets. A total of 18682 gluon jets in Y type events are selected using this single jet tag method.

II. For Mercedes type events both of the quark jets have to be identified by applying cuts to the jet probability variable, as all of the three jets have comparable energy. By demanding that two of the three jets satisfy the condition $P_J < 0.1$, the remaining jet is then considered as the gluon provided its probability value P_J exceeds 0.1. A total of 1196 gluon jets have been identified within Mercedes events using this double jet tag method.

In figure 2, the probability distributions of the jets in Y events are shown separately for normal mixture (see Sec. 2.6), charm- and bottom-quarks as well as for gluons.

2.5.1 Gluon and Quark Jet Purities

The efficiency and purity calculations have been made using events generated by the JETSET 7.3 Monte Carlo [9], tuned to DELPHI data [10], passed through the full simulation program (DELSIM [11, 12]) of the DELPHI detector and the standard DELPHI data reconstruction chain; this requires assigning heavy hadrons to the jets. Even in the Monte Carlo, the assignment of parton flavours to the jets is not unique, as in parton models like JETSET the decay history is interrupted by the build of strings (or clusters in the case of

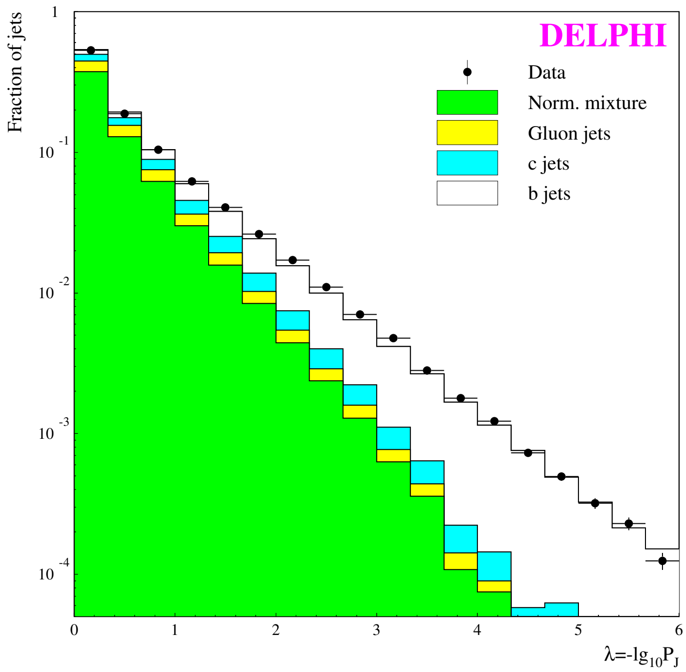

Figure 2: Jet probabilities for normal mixture (in *uds* events), c quark, b quark, and gluon jets (in c and b events)

HERWIG). Thus two independent ways of defining the gluon jet in the fully reconstructed Monte Carlo are investigated [7]. On the one hand it is assumed that the jet which has the largest angle to the heavy hadrons will be the gluon induced jet (angle assignment), on the other hand the jet containing the fewest decay particles from the heavy hadrons is assigned to the gluon (history assignment).

Table 6 shows that the methods give similar results and that therefore the purities can be estimated with small systematic uncertainties. With the tagging procedure described in section 2.5, gluon jet purities [1] of $78.8\% \pm 2.0\%$ (Y events) and $73.2\% \pm 2.5\%$ (Mercedes events) were achieved.

2.6 Corrections

Table 7 shows in detail the fractions of light quarks (*udsc*), b quarks, and gluons of the different jet classes, namely normal mixture jets, b tagged jets and gluon tagged jets in Y events.

The gluon jets are directly compared to a mixed jet sample obtained from all symmetrical three-jet events which have failed the b tag at the event level. This keeps influences of b decays small[2]. The use of subtraction techniques which rely only on the knowledge

[1] Here the purity is defined as the ratio of real tagged gluons (i.e. jets originating from gluons) divided by the number of all jets tagged as gluons.

[2] For simplicity, these are referred to as the 'normal mixture'.

Method		Angle assignment		
	gluon in:	Jet 1	Jet 2	Jet 3
	Jet 1	5.3%	0.05%	0.09%
History	Jet 2	0.01%	34%	0.50%
assignment	Jet 3	0.02%	0.71%	60%

Table 6: Correlation of angle and history assignments. The table has been obtained for arbitrary three-jet events with $\theta_2, \theta_3 \in [110°, 170°]$. These events also contain the Y and the Mercedes events.

Jet Class	light quark content	b quark content	gluon content
normal mixture	47.3%	3.8%	48.8%
b tagged jets	18.7%	61.7%	19.5%
gluon tagged jets	11.7%	9.4%	78.8%

Table 7: Compositions of different jet classes

of the proportion of gluon, light, and b quark jets populating the three-jet event samples enables a comparison of pure light, b quark, and gluon jets.

In the following let R_g, R_l, and R_b be the distributions of any observable for pure gluon jets, for pure light quark jets, and pure b jets, respectively. Then the measured distributions for identified gluon jets ($R_{g_{tag}}$), for tagged b jets ($R_{b_{tag}}$) and for the normal mixture event sample (R_{mix}) can be written as follows:

$$\begin{aligned} R_{mix} &= p^l_{mix} \cdot R_l + p^b_{mix} \cdot R_b + p^g_{mix} \cdot R_g \\ R_{b_{tag}} &= p^l_{b_{tag}} \cdot R_l + p^b_{b_{tag}} \cdot R_b + p^g_{b_{tag}} \cdot R_g \\ R_{g_{tag}} &= p^l_{g_{tag}} \cdot R_l + p^b_{g_{tag}} \cdot R_b + p^g_{g_{tag}} \cdot R_g \end{aligned} \qquad (2)$$

Here the p^j_i are the corresponding fractions from table 7. By solving equation 3 for R_g, R_{q_l} and R_{q_b} one gets the data distributions for pure b quark, light quark and gluon jets.

To correct for limited detector acceptance and resolution, an acceptance correction factor has also been applied.

3 Subjet Properties

The fundamental QCD couplings are illustrated in figure 3. They are determined in terms of the generators t^r_{ab} and the structure constants f^{rst} of $SU(3)$ (in the fundamental description for quarks and in the adjoint description for gluons) by the relations [13]:

$$t^r_{ab} t^r_{bc} = \delta_{ac} C_F$$

$$
\begin{aligned}
f^{rst} f^{rsu} &= \delta_{tu} C_A \\
t^r_{ab} t^s_{ab} &= \delta_{rs} T_F
\end{aligned}
$$

where $a, b, c = 1 \ldots 3$ are quark colour indices and $r, s, t = 1 \ldots 8$ are gluon colour indices, and a sum over repeated indices is implied.

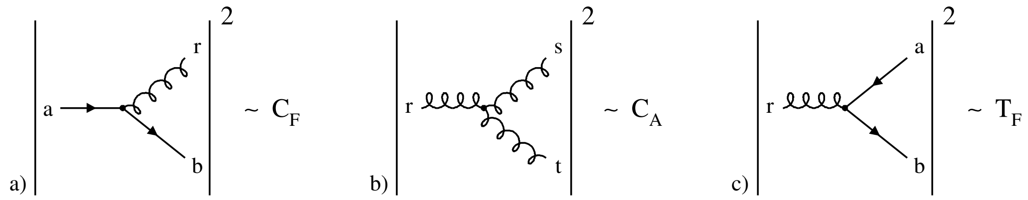

Figure 3: Diagrams of the fundamental QCD couplings

The colour factors (also called Casimir factors) are the eigenvalues of the Casimir operators of $SU(3)$. The Casimir factors C_F, C_A, and T_F determine the coupling strengths of gluon radiation from quarks, of the triple-gluon vertex, and of gluon splitting into a quark-antiquark pair, respectively. Within $SU(3)$, these coupling constants are $C_F = 4/3, C_A = 3$, and $T_F = 1/2$, which has to be weighted by the number of active quark flavors n_F. Due to the quark masses, the actual value of active flavours n_F is energy dependent. At large energy (as e.g. for Y- and Mercedes events), the JETSET model predicts $n_u \sim n_d \sim n_s \sim n_c \sim 2 \cdot n_b$, which corresponds to $n_F \simeq 4.5$, whereas in the low energy limit $n_F \simeq 3$.

3.1 Scale Dependence of the Fragmentation Function of Quark and Gluon Jets

Jet splittings may be studied with respect to the energy sharing in a splitting process. This analysis is connected to the analysis of the scale dependence (scaling violation) of fragmentation functions $D^F_p(x_E, s)$ described by the GDLAP [3] equation [14]. In the limit of large hadron energy fractions $x_E = E_{hadron}/E_{jet}$, i.e. for $x_E \geq \frac{1}{2}$, the lower energy parton in a splitting process cannot contribute. In a $q \to qg$ splitting process the lower energy parton is almost always the gluon. The (leading order) evolution equations for quarks and gluons therefore simplify to:

$$
\frac{dD^F_g(x_E, s)}{d \ln s} = \frac{\alpha_s(s)}{2\pi} \cdot \int_{x_E}^{1} \frac{dy}{y} P_{g \to gg + q\bar{q}}(\frac{x_E}{y}) \cdot D^F_{q/g}(y, s)
$$

[3] **G**ribov, **D**okshitzer, **L**ipatov, **A**ltarelli and **P**arisi

$$\frac{dD_q^F(x_E,s)}{d\ln s} = \frac{\alpha_s(s)}{2\pi}\cdot\int_{x_E}^1 \frac{dy}{y} P_{q\to qg}(\frac{x_E}{y})\cdot D_q^F(y,s)\,.$$

Explicit summation over the gluon splittings is omitted here for simplicity. The Altarelli Parisi splitting probabilities are:

$$\begin{aligned}
P_{q\to qg}(z) &= C_F\cdot\frac{1+z^2}{1-z}\\
P_{g\to q\bar{q}}(z) &= n_F T_F\cdot(z^2+(1-z)^2)\\
P_{g\to gg}(z) &= 2C_A\cdot\frac{(1-z(1-z))^2}{z(1-z)}
\end{aligned}$$

For a quantitative comparison of gluon and quark fragmentation, it is important to compare the relative size of the observed scaling violation:

$$\mathcal{S} = \frac{d\ln D^F}{d\ln s}, \tag{3}$$

where s is the relevant scale. Thus the following ratio is defined:

$$r_{\mathcal{S}}(x) = \frac{\mathcal{S}_g}{\mathcal{S}_q} = \frac{\frac{d\ln D_g^F(x)}{d\ln s}}{\frac{d\ln D_q^F(x)}{d\ln s}}.$$

This ratio can be predicted by solving the GDLAP equation [15]. The limit $r_{\mathcal{S}}(x\to 1)$ is easily calculated:

$$r_{\mathcal{S}}(1) = \lim_{x_E\to 1}\frac{\frac{d\ln D_g^F(x_E,s)}{d\ln s}}{\frac{d\ln D_q^F(x_E,s)}{d\ln s}} = \frac{C_A}{C_F}$$

Thus $r_{\mathcal{S}}$ can be used directly to measure $\frac{C_A}{C_F}$. Experimentally $r_{\mathcal{S}}(x)$ is accessible by measuring the ratio:

$$r_S(x_E) = \frac{S_g(x_E)}{S_q(x_E)}$$

where

$$S_p(x_E) = \frac{D_p^F(x_E,s) - D_p^F(x_E,s_0)}{D_p^F(x_E,s_0)}; \qquad p = q,g$$

The division by $d\ln s$ has been omitted here because later on quark and gluon jets of the same scale are compared.

In e^+e^- - annihilation, large numbers of gluon jets are only available at Z energies. Thus the only possibility to access this information is to compare gluon and quark jets obtained from different three-jet topologies like Y- and Mercedes events. Thus we have to select the relevant scales for the corresponding quark and gluon jets.

In the spirit of first order GDLAP equations and independent fragmentation used throughout this analysis, the only Lorentz invariant observable which may be defined is the transverse momentum or equivalently the invariant mass of a one to two (quark or gluon) splitting process. This scale is also applied in the most commonly used Monte Carlo fragmentation models [9, 16, 17]. However, as in other investigations of scaling violations, this scale is not measured in this study of scaling violations. The transverse momentum of a jet in the preceeding splitting process (e.g the primary $q \to qg$ splitting), however, is easily determined as:

$$\kappa_{2,3} = E_{2,3} \cdot \sin \frac{\theta_1}{2}$$

(Here θ_1 is the angle as defined in fig 1.) κ is also called hardness of the splitting. As only the relative change of the scale matters, and the transverse momentum of the splitting process under study should be proportional to this, we use the hardness κ as the scale. This choice is completely analogous to the choice of the centre of mass energy as the scale in the traditional studies of scaling violations.

3.2 Subjet Rates

Differences in the splitting properties of quarks and gluons are expected to appear most clearly in the "first" splitting process at large momentum transfer or jet resolution parameter y. To study the splitting processes in jets into subjets (which was not investigated in previous analyses [18, 19]), the jet algorithm used for the subjet definition has been applied only to those particles which have, at the event level, been assigned to the jet under study [7] (see Fig. 4 for the definition of a subjet).

This strategy should result in a more meaningful comparison of the y values of individual jets as the experimental smearing due to the energy normalization is smaller.

The absolute splitting rate of a jet $\Delta N_1(y)$ should be proportional to the number of unsplit jets $N_1(y)$ present at given jet resolution y; to some dynamical expression $\mathcal{F}(y)$ containing in particular the coupling constant and the colour factors of the relevant parton initiating the jet; and to the size of the y interval Δy, i.e.

$$\Delta N_1(y) = -\mathcal{F}(y) \cdot N_1(y) \cdot \Delta y$$

This expression is analogous to the radiative decay equation with a y dependent decay probability $\mathcal{F}(y)$. Thus the *modified differential one jet rate* $\tilde{D}_1(y)$ defined as [4] :

$$\tilde{D}_1(y) = \frac{1}{N_1(y)} \cdot \frac{\Delta N_1(y)}{\Delta y} = -\mathcal{F}(y)$$

is a direct measure of the differential jet decay or splitting probability density $\mathcal{F}(y)$. Using the conventional definition of the jet rate:

$$R_1(y) = \frac{N_1(y)}{N_{tot}}$$

where N_{tot} is the total number of jets to start with and $N_1(y)$ is the number of surviving "1-jets" at a fixed scale, one obtains:

[4] The symbol D is used in this paper for both differential jet rates, and for structure functions

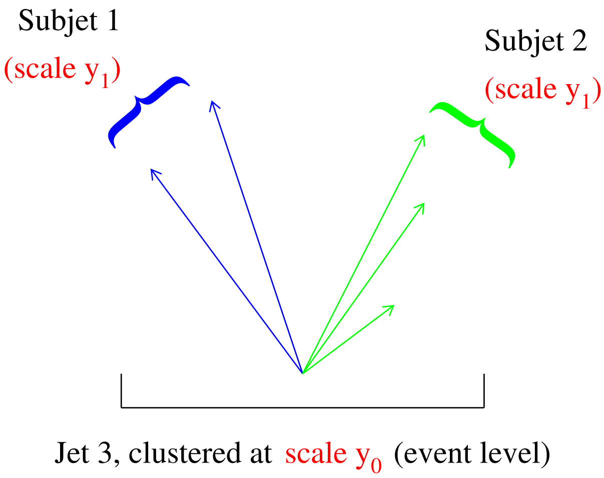

Figure 4: Definition of a subjet.

$$\tilde{D}_1(y) = \frac{1}{R_1(y)} \cdot \frac{R_1(y) - R_1(y - \Delta y)}{\Delta y} \approx \frac{d \ln R_1(y)}{dy}$$

Note that this definition has the same formal structure as the scaling violation defined in equation 3. A similar approach is used in parton shower simulations [20].

$\tilde{D}_1(y)$ differs from the usual definition of the differential jet rate $D_1(y)$ [21] by the extra factor $1/R_1$. This definition can be generalized also to higher rank (second, third ...) splittings yielding for the n'th splitting:

$$\tilde{D}_n(y) = \frac{1}{R_n(y)} \cdot \frac{R_n(y) - R_n(y - \Delta y)}{\Delta y} + \frac{R_{n-1}(y)}{R_n(y)} \cdot \tilde{D}_{n-1}(y)$$

Here the (sub-) jet rates $R_n(y)$ are defined as usual by $R_n = N_n(y)/N_{tot}$, where $N_n(y)$ is the number of jets in which $n-1$ splittings occurred up to the given jet resolution y.

The modified differential jet rates $\tilde{D}_n(y)$ measured at different values of y are by construction uncorrelated, in contrast to the jet rates R_n or the average subjet multiplicities. $\tilde{D}_1$ or $\mathcal{F}(y)$ should in principle be calculable perturbatively if jets are defined using an infrared and collinear safe jet algorithm, as for example the Durham algorithm [8].

The modified differential jet rates can be measured individually for quark and gluon jets. Naïvely, assuming that the divergent bremsstrahlung terms in the Altarelli-Parisi splitting functions dominate, it should be expected that the gluon to quark ratio $\tilde{r}_1$ should depend mainly on the colour factors C_A and C_F:

$$\tilde{r}_1 = \frac{\tilde{D}_1^g}{\tilde{D}_1^q} = \frac{C_A + \eta n_F T_f}{C_F} \tag{4}$$

The term $\eta n_F T_f (0 \leq \eta \leq 1)$ accounts for the non-divergent contribution of the $g \to q\bar{q}$ splitting. Heavy quark production in gluon splitting is expected to be suppressed, yielding $n_F \approx 4.5$ within the JETSET model for the topologies considered. Numerically, allowing the full range for η, of 0 to 1, one expects $\tilde{r}_1 = 2.25 - 4.0$.

4 Results

4.1 Scale Dependence of the Fragmentation Functions

Sizeable differences have been observed between the scaled energy x_E-distributions of stable hadrons produced in quark and gluon jets [4, 22, 23]. Fig. 5a,b show the scaled energy distributions of charged hadrons for quark and gluon jets [5].

The quark fragmentation functions in Y- and Mercedes events are in good agreement with those measured from all events at lower energies [24]. We compare to data at beam energies similar to the hardness κ of jets in three-jet events, as the energy spectra and other characteristics of the QCD partonic cascade are expected to mainly depend on the hardness of the corresponding jet [25]. The agreement is far less satisfactory if the quark fragmentation function measured from Y and Mercedes events is compared to the overall e^+e^- data at similar jet energy.

An approximately exponential decrease of the fragmentation function with increasing x_E is seen, which is more pronounced in the gluon case. The extra suppression at high x_E (by almost one order of magnitude) of gluon jets relative to quark jets is expected because, contrary to the quark case, the gluon cannot be present as a valence parton inside the produced hadron. The valence quarks of the hadrons first have to be produced in a $g \to q\bar{q}$ splitting process.

To demonstrate the scale dependence, figure 5c shows the x_E-distributions as obtained at different CMS energies [24] and from light quark and gluon jets in Y- and Mercedes events.

It is observed that the distributions measured from the higher energy jets in Mercedes events show a stronger fall off with hadron energy than for the lower energy jets from Y events. This is similar to the behaviour of scaled energy distributions measured at different centre of mass energies [24]. More quantitatively, figure 6 shows the relative change S of the stable hadron fragmentation function at two different jet energies with a change in $\log(E_beam)$ corresponding to the change of $\log(\kappa)$ for Y- and Mercedes events.

Figure 6a compares S_e as measured from all events at PETRA, $E_{jet} \approx 11$ GeV and $E_{jet} \approx 22$ GeV [24], to S_q for quark jets in Y- and Mercedes events, which have similar values of κ, i.e. jets of $\kappa = 12$ GeV and 26 GeV, respectively. The typical pattern expected from scaling violation, a depletion at large energy and an increase at small energy, is observed. The scale dependence vanishes for $x_E \approx 0.1$. The behaviour of S_e and S_q is similar and for large x_E they are consistent within errors. For very small scaled energy x_E, some discrepancies are expected due to the mis-assignment of particles to a jet in three-jet events.

[5]This figure is similar to a figure shown in [4] but now also includes the data collected in 1994.

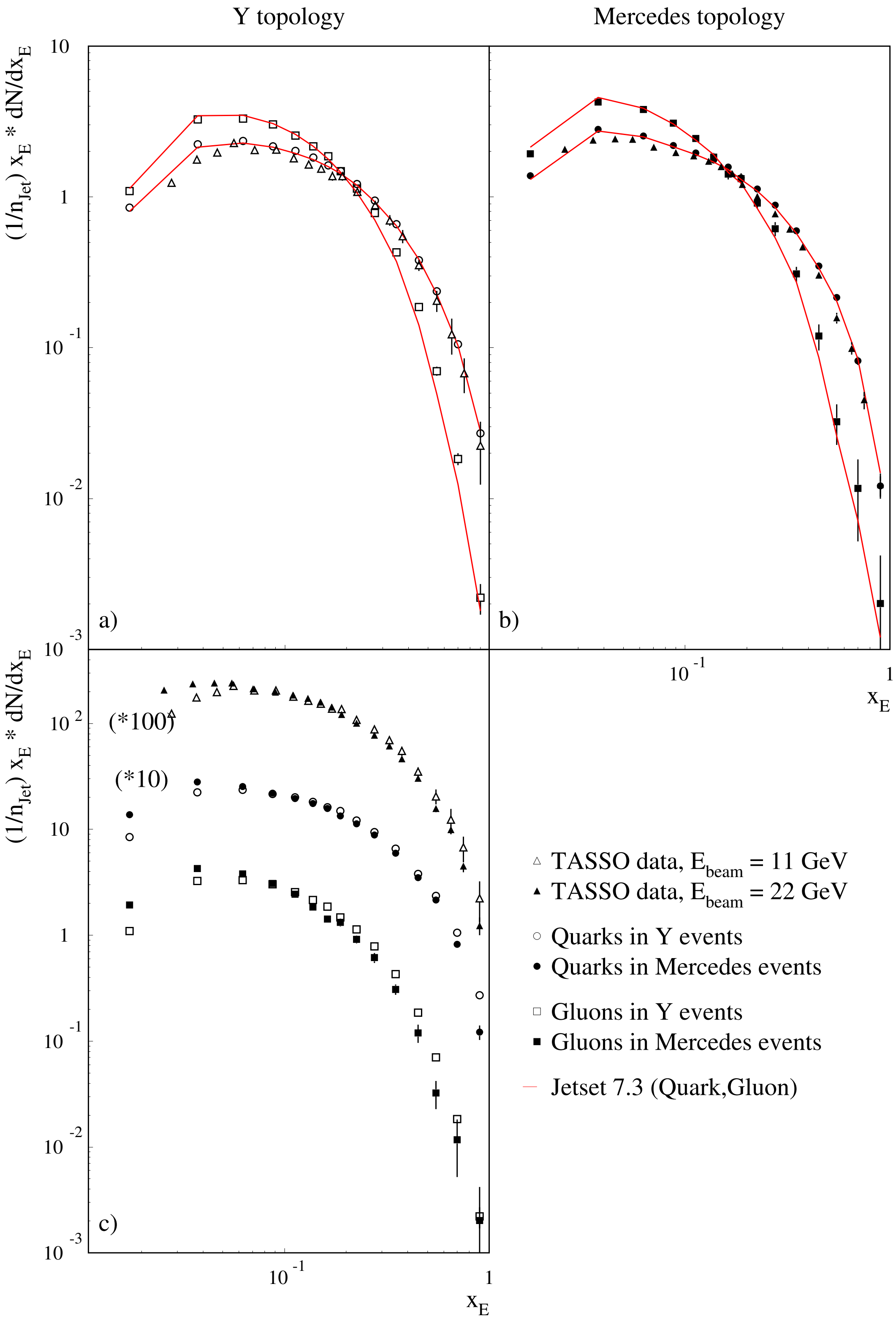

Figure 5: Scaled energy distributions for Y and Mercedes type events; the solid lines are the corresponding JETSET 7.3 Monte Carlo predictions. TASSO data are obtained from all events scaled by $\frac{1}{2}$, because most of the events are two-jet events.

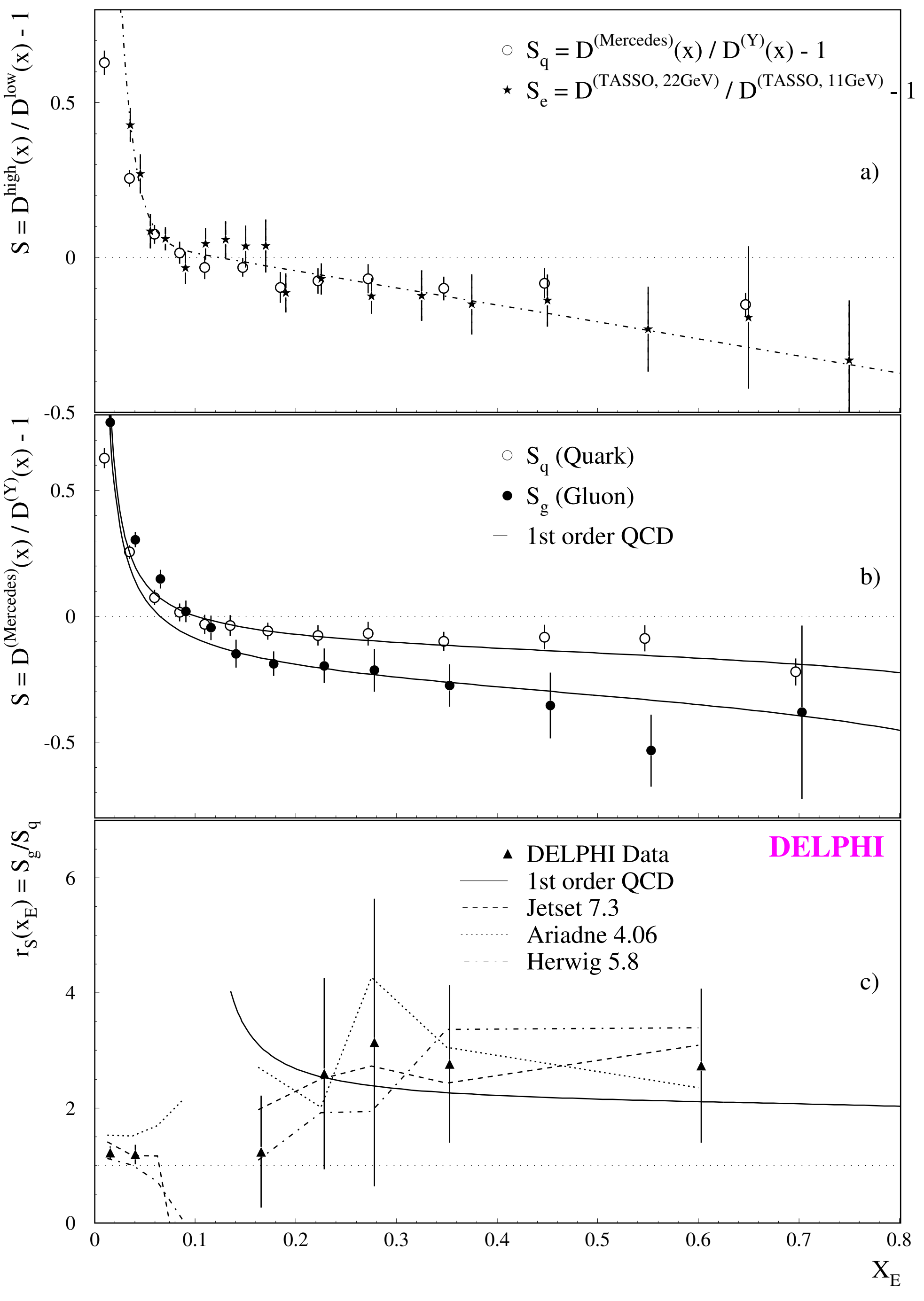

Figure 6: The upper plot shows the ratio S of quark fragmentation functions at different energies. The line is a fit to the DELPHI/TASSO data. The second plot compares S_q to S_g and the last figure represents the ratio $\frac{S_g}{S_q}$.

In figure 6b the relative change S_q for quark jets and the corresponding change S_g for gluon jets are compared. For gluon jets the typical scaling violation pattern is also observed. It is significantly more pronounced than for quark jets, which is to be expected owing to the higher gluon splitting probability. The scale dependence vanishes for $x_E \approx 0.1$ as well. To our knowledge this is the first direct observation of scaling violations in identified gluon jets and confirms our conjecture raised in a previous publication [4].

In figure 6c the ratio $r_S(x_E) = S_g(x_E)/S_q(x_E)$ is shown, which differs from 1 at small and large x_E. At small x_E, this is due to the multiplicity increase with energy which is more pronounced in gluon than in quark jets [4]. For $x_E \approx 0.1$, $r_S(x_E)$ is undefined experimentally because both S_g and S_q vanish there. At large x_E, $r_S(x_E)$ increases and rapidly approaches values around two. Averaging over $r_S(x_E)$ for $x_E > 0.2$ yields

$$r_S(0.2 \leq x_E \leq 0.8) = 2.8 \pm 0.8_{stat}.$$

Thus we observe a large ratio of splitting probabilities in quark and gluon jets, consistent with the expected ratio $r_S(x_E) = C_A/C_F = 9/4$.

It should be noted that due to the stronger scaling violations in gluon jets compared to quark jets, the hadron multiplicity in gluon jets increases faster with increasing hardness or energy. Thus scaling violations explain at least in part the observed increase of the multiplicity ratio in gluon and quark jets with energy [4].

4.2 Subjet Splittings

The modified differential jet rates $\tilde{D}_n(y)$, the differential jet rates $D_n(y)$ and the jet rates $R_n(y)$ have been measured in Y- and Mercedes events. The results are presented in figure 7 for Y events.

Figure 7a, shows a comparison of $\tilde{D}_1(y)$ for quark and gluon jets. For large y, $\tilde{D}_1^g(y)$ is smaller than $\tilde{D}_1^q(y)$ (open circles), confirming the QCD prediction that the splitting probability of gluons is larger than for quarks.

For quantitative comparison the uppermost points in figure 8a show the ratio $\tilde{r}_1(y)$ of the gluon and quark differential splitting probabilities $\tilde{D}_1^{g/q}(y)$. A bump structure is observed with a maximum at $\log y \approx -1.7$. The maximum values are given in table 8. The ratio agrees well with the naïve QCD expectation as given by the colour factors (Eqn. 4). The bump is also present in the parton shower simulations performed with JETSET [9], HERWIG [17] or ARIADNE [16] (see Fig. 9). Some discrepancies among the models are visible. JETSET agrees best with the data.

The depletion of $\tilde{r}_1(y)$ at large y indicates a suppression of the initial splitting of gluon jets. Owing to the choice of symmetric Y events, it is clear that this suppression is of dynamical nature and cannot be due to phase space effects. Moreover it is at large y where interference effects are expected to occur most likely. The properties of this suppression are further studied in Sec. 4.3.

It is instructive to study further the behaviour of $\tilde{D}_1^g(y)$. At smaller y ($\log y < -3$), $\tilde{D}_1^g(y)$ falls off because almost all gluon jets have already split whereas $\tilde{D}_1^q(y)$ still rises until $\log y < -3.5$ [6]. Here also almost no non-split quark jets are left and $\tilde{D}_1^q(y)$ drops to zero. Thus for $\log y < -3$ the ratio $\tilde{r}_1(y)$ (compare figure 8) is smaller than 1.

[6] Recall that the $\tilde{D}$ are properly normalized probability densities.

ratio	Y events		Mercedes events		Average		QCD colour factor
	data	**Jetset PS**	**data**	**Jetset PS**	**data**	**Jetset Ps**	**expectation**
$\tilde{r}_1^{max}$	3.18 ± 0.18	3.66 ± 0.08	2.67 ± 0.31	3.12 ± 0.10	3.05 ± 0.16	3.45 ± 0.06	2.25 - 4

Table 8: Ratio of the modified differential one jet-rate for Y- and Mercedes events (data and simulation) at the maximum

The higher differential splitting probabilities $\tilde{D}_2, \tilde{D}_3$ and $\tilde{D}_4$ are shown in the lower rows of Fig. 7a. Differences between quarks and gluons become smaller with increasing splitting rank n and almost vanish already for $\tilde{D}_4$. This is also seen in the evolution of the ratio $\tilde{r}_n(y)$ with n (see figure 8a). For $n \geq 4$ the $\tilde{r}$ are almost unity. This is understood because of the sizable number of gluons in both types of jets. The only difference remaining is the initial quark. In other words each jet is predominantly a "gluon jet". For completeness we show in Fig. 7c the absolute subjet rates R_i.

The higher splitting probability $\tilde{D}_1$ in quark jets at low y (as compared with gluon jets) leads to a compensation of the initially higher subjet rate D_1 in gluon jets. This mechanism also holds for the higher jet rates D_2 to D_4, contrary to the behaviour of the $\tilde{D}_n$ distributions, and is again most clearly seen in the corresponding ratios (see figure 8). The difference of the behaviour of the $\tilde{D}_n$ and D_n distributions is due to the different number of quark and gluon initiated jets (with n subjets) present at a given y which are able to split into $n+1$ subjets. This compensation and the initial suppression of gluon splittings are presumably responsible for the relatively small stable hadron multiplicity ratio of ≈ 1.25 observed from gluon and quark jets in three-jet events at LEP energies [4].

It has been checked that Mercedes events yield similar, although statistically less significant, results. Especially the suppression of $\tilde{r}_1$ at large y is also present.

The angles between the quark and gluon jets in Mercedes events are not too different from events with very high energy gluons which have been analysed in a recent publication [5]. Thus it is expected that even in these events the observed suppression takes place, and is the main cause of suppressing the multiplicity ratio for gluon to quark jets observed even for these high energy gluons.

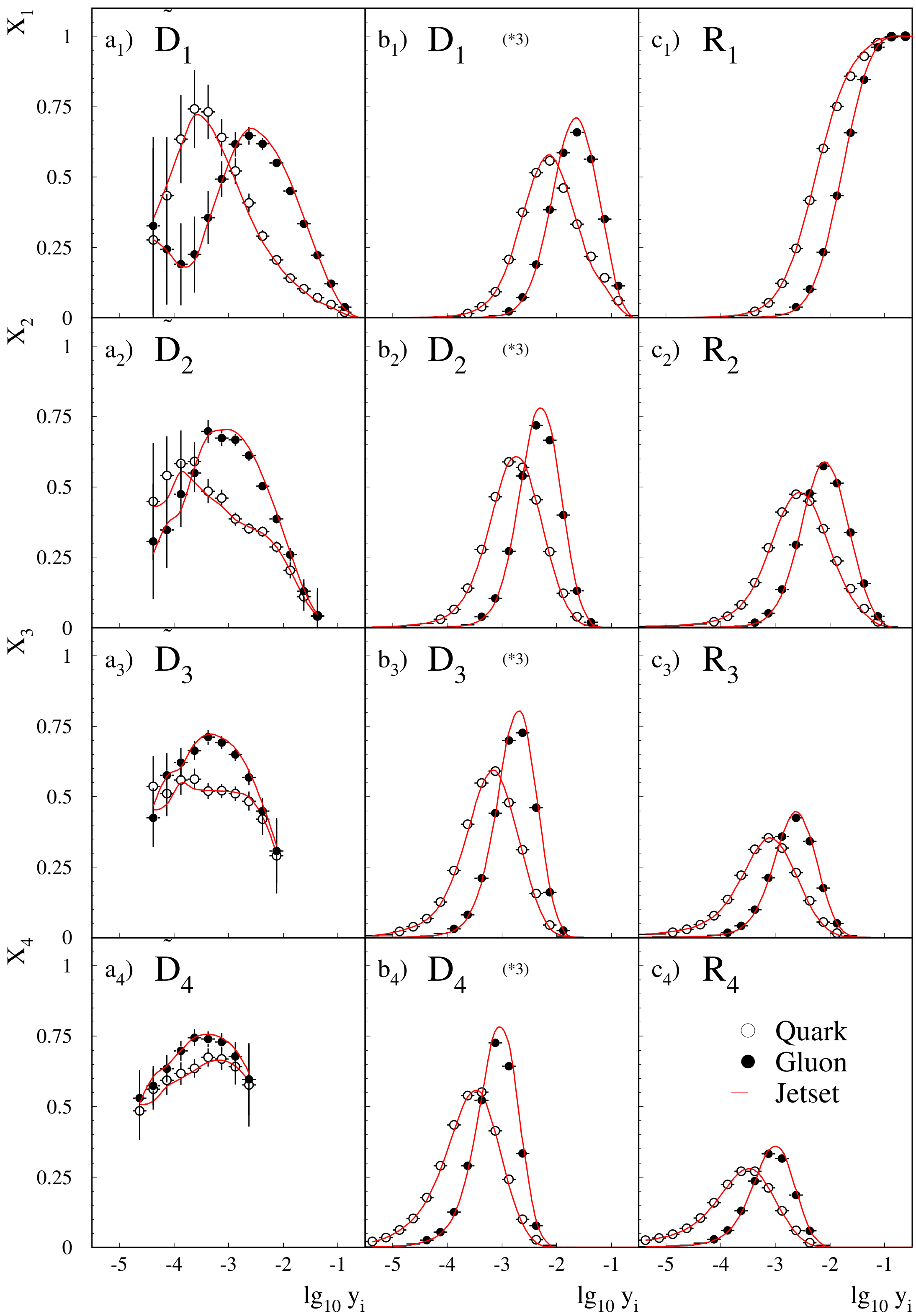

Figure 7: Jet rates ($\tilde{D}_i^{q,g}$,$D_i^{q,g}$,$R_i^{q,g}$) in Υ events. Here X_i denotes $\tilde{D}_i$, D_i or R_i.

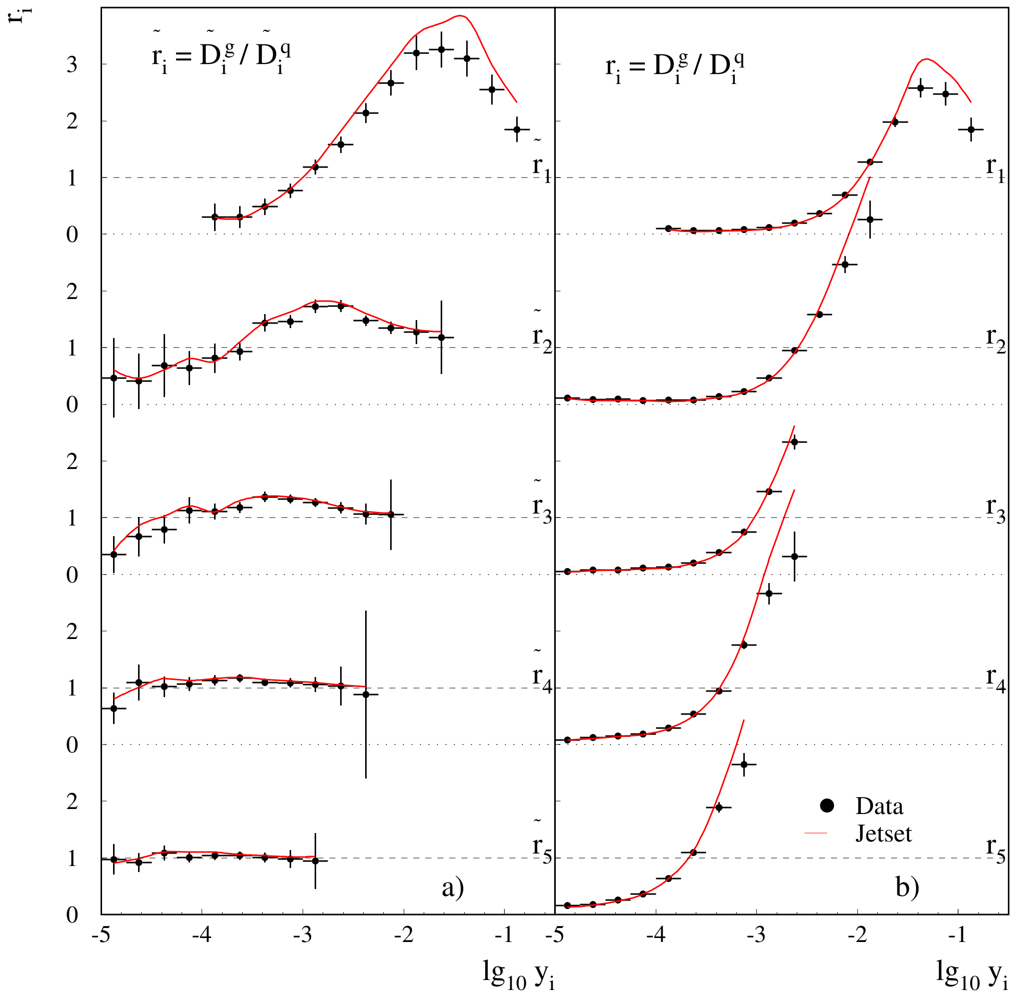

Figure 8: Ratios of the modified differential jet rates ($\tilde{r}_i = \tilde{D}_i^g/\tilde{D}_i^q$) and the differential jet rates ($r_i = D_i^g/D_i^q$) in Υ events

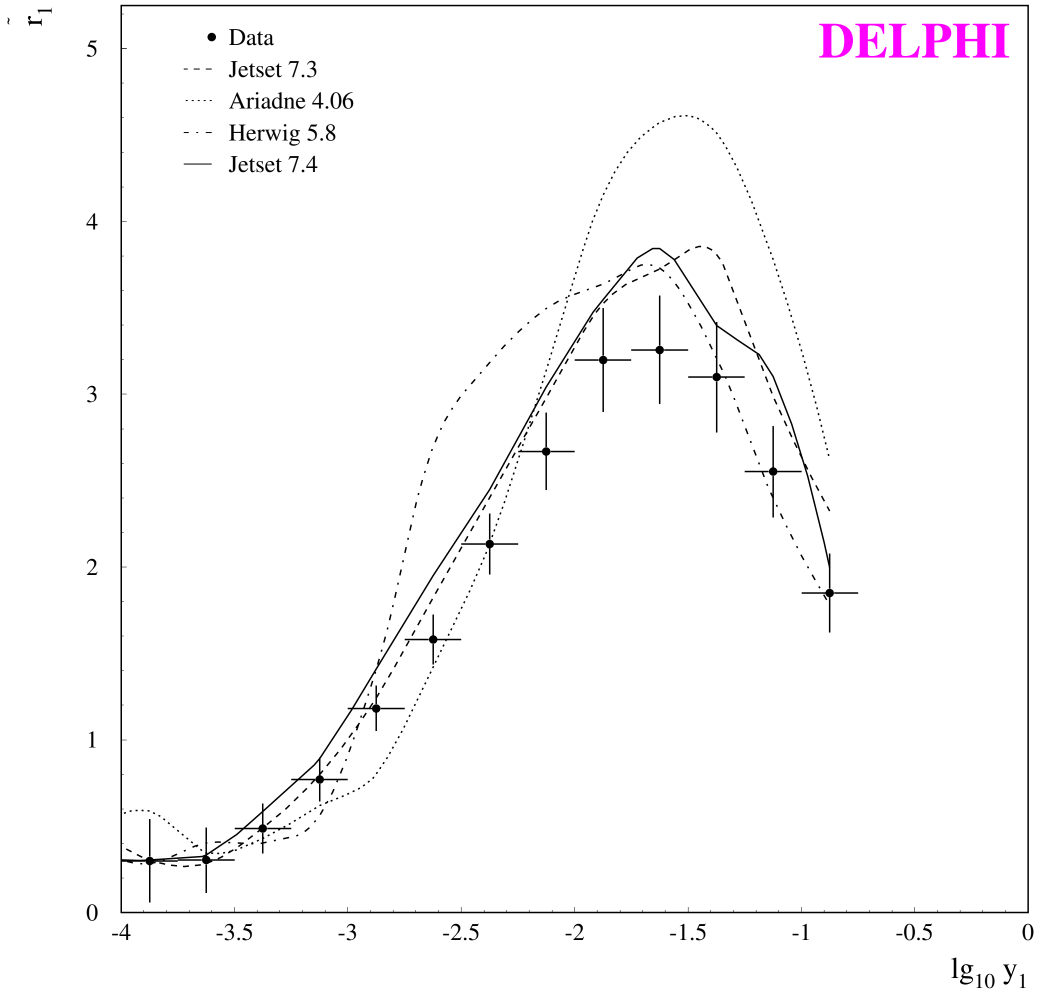

Figure 9: Comparison of $\tilde{r}_1$ to different Monte Carlo generator predictions

4.3 Asymmetry of the Subjet Azimuthal Distribution

At large y a suppression of the gluon splitting probability was observed. To further investigate the properties of this suppression we study the azimuthal distribution with respect to the event plane. Specific azimuthal distributions may be expected in the presence of interference effects.

To explain the observables of this measurement, Fig. 10 sketches a Y event including a quark and a gluon splitting process.

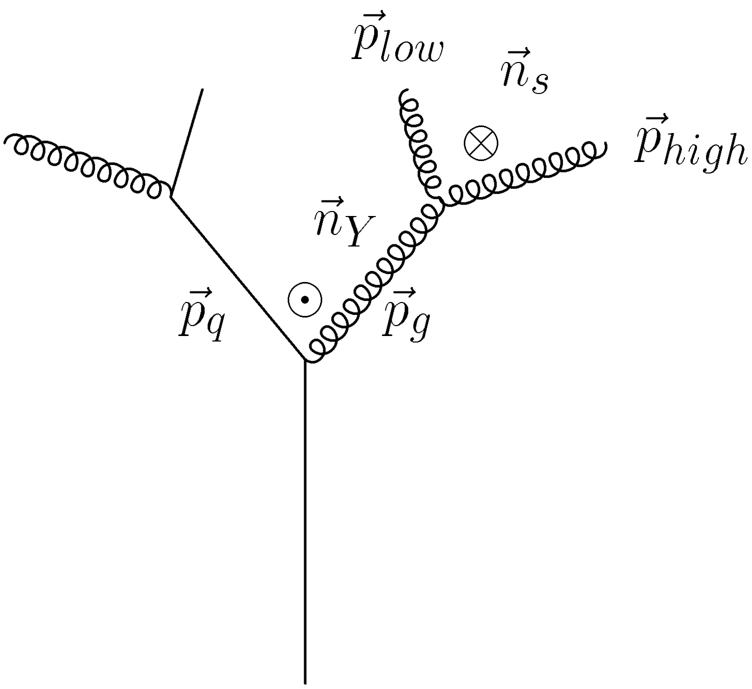

Figure 10: Illustration of subjet angles. For the normal mixture sample one has to replace $\vec{p}_g$ and $\vec{q}_g$ by the corresponding relevant jets.

The normals of the event plane $\vec{n}_Y$ and the subjet plane $\vec{n}_S$ are defined by:

$$\begin{aligned}\vec{n}_Y &= \frac{\vec{p}_g \times \vec{p}_q}{p_g \cdot p_q} \\ \vec{n}_S &= \frac{\vec{p}_{low} \times \vec{p}_{high}}{p_{low} \cdot p_{high}}\end{aligned}$$

respectively. When the splittings of the quark jet are considered the direction of $\vec{n}_Y$ is inverted taking into account the 180° difference in azimuth between the gluon and the quark.

The distribution of the azimuthal angle Ψ between the normal vectors $\vec{n}_S$ and $\vec{n}_Y$ for quark and gluon jets is shown in Fig 11a.

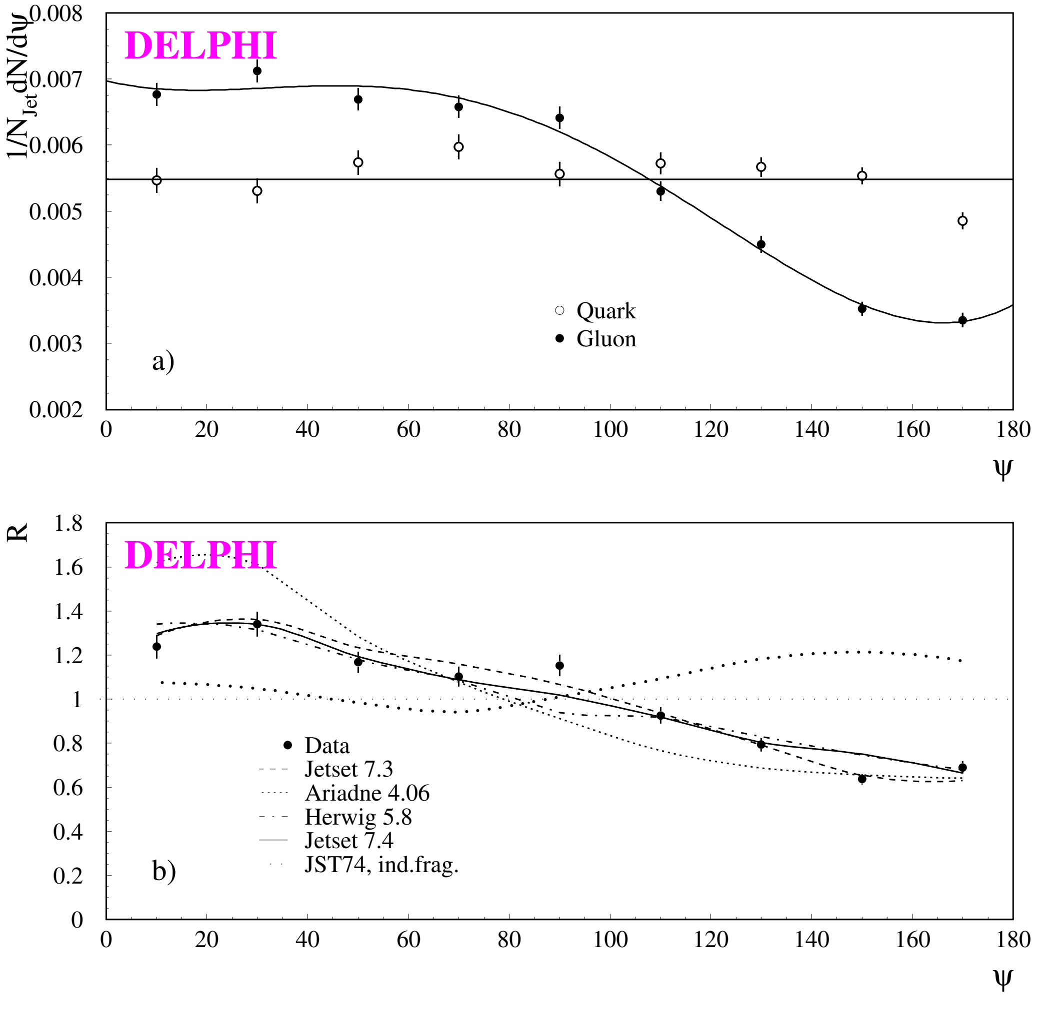

Figure 11: Comparison of subjet azimuthal angles for quark jets and for gluon jets (a), and the comparison of the corresponding ratio with predictions of various Monte Carlo models (b). The lines in (a) are to guide the eye.

For the quark jet the Ψ distribution is almost flat. For the gluon jet, however, a strong depletion is observed at $\Psi = 180°$ and an obvious excess at $\Psi = 0$. This implies that the more energetic subjet from a gluon splitting is emitted dominantly to the inside of the Y (i.e. opposite to the situation in fig 10). When studying the azimuthal distribution as a function of y, it is found that the depletion almost vanishes for small y but is very strong for large y. Thus at large y the splittings occur only in part of the available Ψ interval.

In Fig 11b the ratio of the gluon to quark azimuthal distribution is compared to the expectation of various fragmentation models. The models including coherence effects quantitatively describe the observed behaviour of this distribution, as well as the individual quark and gluon distributions in Fig 11a (model distributions not shown). In contrast, the JETSET model with coherence effects switched off and independent fragmentation ($mstj(1) = 2, mstj(2) = 3, mstj(3) = 1$ and $mstj(42) = 1, mstj(44) = 1$) however predicts essentially a flat behaviour for this ratio [7]. This may be taken as indication that interference effects cause the observed depletion.

From the behaviour of the Ψ distribution for gluon jets, it is seen that only a part of the available phase space for gluon splitting is actually populated. Therefore the initial ratio of the subjet multiplicity in gluon jets with respect to quark jets is diminished. As this ratio is essentially preserved in the further jet evolution (as is shown in Sec. 4.2), this explains why the multiplicity ratio in gluon and quark jets is not larger.

5 Conclusions

Light quark and gluon jets of similar energy have been selected from planar symmetrical three-jet events measured with DELPHI. Using impact parameter techniques, gluon jets have been selected in heavy quark events, and heavy quark contributions have been depleted in a mixed quark/gluon jet sample. Properties of pure quark and gluon jets have been obtained by the technique decribed in section 2.6.

Jet splitting has been studied using the scale dependence of the quark and gluon fragmentation functions. Y- and Mercedes events provide sources of quark and gluon jets of different energy (on average 24 GeV and 30 GeV, respectively). The scale dependence of the fragmentation function measured in quark jets shows the typical scaling violation pattern as observed from all events at different centre-of-mass energies. For the first time scaling violations have been observed in identified gluon jets. At large hadron energies $x_E > 0.2$, the ratio of the relative change of the fragmentation function for quarks and gluons is measured to be:

$$r_S(0.2 \leq x_E \leq 0.8) = 2.8 \pm 0.8_{stat.}$$

This value is of comparable size with the QCD expectation $r_S(x_E \to 1) = C_A/C_F = 9/4$ and confirms that the ratio of gluon to quark splitting is controlled mainly by the colour factors. The scale dependence of the ratio of the hadron multiplicity in quark and gluon jets at least in part is due to the observed scaling violations.

This finding has been confirmed by studying the differential subjet splitting probabilities $\tilde{D}_p(y)$ which are introduced in section 3.2. The maximum of ratio of the first splitting probabilities in quark and gluon jets is measured to be:

$$\tilde{r}_1 = 3.18 \pm 0.18_{stat.}$$

This agrees with the expectation from fragmentation models and is consistent with the naïve expectation (see Eqn. 4).

The study of higher rank splittings in quark and gluon jets leads to the conclusion that the initially higher subjet rate in gluon jets is compensated at smaller y by a larger differential splitting rate D_1 in quark jets. This phenomenon is consistently observed up to the 5'th rank splitting.

At large y the subjet splitting probability $\tilde{D}_1$ is suppressed. This is found to be due to an azimuthal angle asymmetry of the normal of the subjet plane with respect to the

[7] Independent fragmentation is used as in other analyses [28], as it is known that string fragmentation mimics coherence effects.

event plane. No asymmetry is observed for quark jets. This behaviour is also predicted by Monte Carlo models including coherence effects.

This suppression in connection with the observed further jet evolution causes the small observed hadron multiplicity ratio in gluon to quark jets in three-jet events in e^+e^- - annihilation.

Acknowledgements

We are greatly indebted to our technical collaborators and to the funding agencies for their support in building and operating the DELPHI detector, and to the members of the CERN-SL Division for the excellent performance of the LEP collider. We also thank Yu.L. Dokshitzer, T. Sjöstrand, S. Catani and P. Kroll for useful and illuminating discussions.

References

[1] S.J. Brodsky, J. Gunion, Phys. Rev. Lett. **37** (1976) 402;
K. Konishi, A. Ukawa, G. Veneziano, Phys. Lett. **B78** (1978) 243.

[2] A.H. Mueller, Nucl. Phys. **B241** (1984) 109;
J.B. Gaffney, A.H. Mueller, Nucl. Phys. **B250** (1985) 109;
E.D. Malaza, B.R. Webber, Phys. Lett. **B149** (1984) 501;
E.D. Malaza, Zeit. Phys. **C31** (1986) 143;
I.M. Dremin, R.C. Hwa, Phys. Lett. **B324** (1994) 477;
I.M. Dremin, V.A. Nechitailo, Modern Phys. Lett. **A9** (1994) 1471.

[3] OPAL Collaboration, Z. Phys. **C58** (1993) 387;
OPAL Collaboration, Z. Phys. **C68** (1995) 179;
ALEPH Collaboration, Phys. Lett. **B313** (1993) 535;
ALEPH Collaboration, Phys. Lett. **B384** (1996) 353.

[4] DELPHI Collaboration, Z. Phys. **C** 70 (1996) 179.

[5] OPAL Collaboration, CERN-PPE/96-116.

[6] DELPHI Collaboration, Nucl. Instr. and Methods in Physics Research **A303** (1991) 233.

[7] O. Klapp, Diplomarbeit "Quark- und Gluonjets aus Z-Zerfällen — Vergleichende Studien des Jetendzustandes und der Substruktur" WU **D** 95-15 (University of Wuppertal, Germany).

[8] S. Catani, Yu.L. Dokshitzer, M. Olsson, G. Turnrock, B.R. Webber, Phys. Lett. **B269** (1991) 432;
S. Bethke, Z. Kunszt, D.E. Soper, W.J. Stirling, Nuclear Physics **B370** (1992) 310.

[9] T. Sjöstrand, Comp. Phys. Comm. **39** (1986) 346;
T. Sjöstrand, M. Bengtsson, Comp. Phys. Comm. **43** (1987) 367;
T. Sjöstrand, *JETSET 7.3 Program and Manual*, CERN-TH 6488/92.

[10] DELPHI Collaboration, CERN-PPE-96-120, Submitted to Z. Phys. C.

[11] The DELPHI Collaboration, *DELPHI event generation and detector simulation*, DELPHI 89-67 PROG-142.

[12] DELPHI Coll., Nucl. Inst. and Meth. **A378** (1996) 57.

[13] W. Greiner, B. Mueller, Theoretische Physik Band 5, *Quantenmechanik Teil 2, Symmetrien* Verlag Harry Deutsch Thun / Frankfurt a. Main (1990);
T. Hebbeker, Phys. Rep. **217** (1992) 69.

[14] G. Altarelli and G. Parisi, Nucl. Phys. **B126** (1977) 298;
Yu.L. Dokshitzer, Sov. Phys. JETP **46** (1977) 641.

[15] P. Nason and B.R. Webber, Nucl. Phys. **B421** (1994) 473.

[16] L. Loennblad, *ARIADNE 4.4 Program and Manual*, Comp. Phys. Comm. **71** (1992) 15.

[17] G. Marchesini and B.R. Webber, Nucl. Phys. **B283** (1984) 1;
B.R. Webber, Nucl. Phys. **B283** (1984) 492.

[18] ALEPH Collaboration, Phys. Lett. **B346** (1995) 389.

[19] OPAL Collaboration, Z. Phys. **C63** (1994) 363.

[20] T. Sjöstrand, Phys. Lett. **B157** (1985) 321.

[21] L. Smolik, PhD thesis, Heidelberg (1990), DESY-90-089;
DELPHI Collaboration,Zeit. Phys. **C54** (1992) 55.

[22] OPAL Collaboration, Z. Phys. **C68** (1995) 179.

[23] ALEPH Collaboration, Phys. Lett. **B384** (1996) 353.

[24] TASSO Coll., Z. Phys. **C47** (1990) 187.

[25] Yu.L. Dokshitzer, private communication;
Yu.L. Dokshitzer, V.A.Khoze, A.H. Mueller and S.I. Troyan, *Basics of perturbative QCD*, Editions Frontieres, 1991;
Yu.L. Dokshitzer, D.I. Dyakonov and S.I. Troyan, Phys. Reports **58** No. 5 (1980) 269.

[26] Z. Kunszt, P. Nason, G. Marchesini, B.R. Webber, *QCD in Z Physics at LEP 1*, Vol. 1, CERN Report 89-09 (1989).

[27] T. Hebbeker, Phys. Rep. **217** (1992) 69.

[28] A. Para, *Probing QCD with vector Bosons*, Talk presented at the XXVIII International Conference on High Energy Physics, 25-31 July 1996, Warsaw, Poland;
D0 Collaboration, *Color Coherence Effects in Multi-Jet and W+Jet Events at D0*, submitted to the XXVIII International Conference on High Energy Physics, Warsaw, Poland (1996);
L3 Collaboration, Phys. Lett. **B353** (1995) 136.